## **CONFERENCE PRE-PRINT**

# LAGRANGIAN STATISTICS OF HEAVY IMPURITY TRANSPORT IN DRIFT-WAVE TURBULENCE

Zetao Lin Aix-Marseille Université, CNRS, I2M Marseille, France

Email: zetao.lin@etu.univ-amu.fr

Benjamin Kadoch Aix-Marseille Université, CNRS, IUSTI Marseille, France Email: benjamin.kadoch@univ-amu.fr

Sadruddin Benkadda Aix-Marseille Université, CNRS, PIIM Marseille, France Email: saddrudin.benkadda@univ-amu.fr

Kai Schneider Aix-Marseille Université, CNRS, I2M Marseille, France

Email: kai.schneider@univ-amu.fr

# Abstract

The paper analyzes the behavior of tungsten impurities with finite inertia in drift-wave turbulence through the Hasegawa-Wakatani model. Unlike earlier tracer-based models, the simulations indicate a shift to non-diffusive dynamics for a range of charge states. This new mechanism presents a turbulence-driven path to core impurity accumulation, emphasizing the impact of particle inertia on impurity dynamics, which has important implications for impurity control in future fusion devices like ITER.

### 1. INTRODUCTION

Impurities play complex roles in fusion plasmas, influencing both device performance and operational stability. The impurity accumulation within the plasma core can lead to increased radiation, fuel dilution, and consequently, a decline in both energy retention and fusion output [1, 2, 3, 4]. Therefore, gaining a comprehensive understanding of impurity transport is essential for improving the operation of magnetic confinement fusion systems. In tokamaks and similar devices, transport behavior generally manifests anomalous transport instead of classical collision-driven processes [5, 6, 7]. Self-Organized Criticality (SOC) serves as a model to explain these dynamics, characterizing transport as avalanche-type occurrences with non-local connections and long-lasting effects. The SOC-like behavior in both computational and experimental contexts has been thoroughly examined [8]. Within the SOC paradigm, non-diffusive transport in plasma turbulence is often associated with conditions near criticality or the existence of strong, sheared zonal flows [9]. This paper introduces a novel process for non-diffusive transport. Through the analysis of impurity paths in a supermarginal Hasegawa-Wakatani system, we present quantitative data showing that inertia can shift transport from diffusive to non-diffusive, uncovering an overlooked mechanism contributing to the core accumulation of tungsten in ITER-like plasmas.

In the edge regions of tokamaks, drift-wave turbulence primarily governs the turbulent transport of particles and heat [7]. The Hasegawa-Wakatani (HW) model serves as an effective approach for studying drift-wave turbulence, due to its theoretical soundness and computational practicality [10, 11, 12]. Nonetheless, there is a gap in the current plasma physics literature concerning the behavior of impurities with finite inertia when analyzed within the HW framework. Previous studies have explored the dynamics of passive tracers in plasma turbulence but have largely overlooked the impact of inertia [13, 14]. While the significance of particle inertia in driving complex transport phenomena is well-documented in classical fluid dynamics, its implications within plasma turbulence remain insufficiently addressed. This zero-inertia assumption becomes problematic in the context of next-generation fusion reactors such as ITER, where heavy impurities like tungsten will be critical. To bridge this research gap, we present a detailed numerical investigation of impurity transport in HW drift-wave turbulence, explicitly considering particle inertia. Our study systematically assesses transport behaviors across various Stokes numbers by employing a one-way coupling between the turbulent plasma flow and impurity particles. We utilize Lagrangian tracking for individual impurity particles using a drag-based formulation. We suggest that inertial effects lead to a delayed response of heavy impurities to the plasma flow, resulting in a distinctive "lag" effect.

### 2. MODELS FOR SIMULATION

# 2.1. Hasegawa-Wakatani model

For simulating the turbulent environment, plasma fields are produced by numerically solving the two-dimensional HW equations in a slab geometry. These equations capture the fundamental physics of electrostatic potential  $\phi$  and density fluctuations n at the edge region of a tokamak [10, 15]:

$$\left(\frac{\partial}{\partial t} - \mu_{\nu} \nabla^{2}\right) \nabla^{2} \phi = \left[\nabla^{2} \phi, \phi\right] + c(\phi - n) \tag{1}$$

$$\left(\frac{\partial}{\partial t} - \mu_D \nabla^2\right) n = [n, \phi] - \Gamma \frac{\partial \phi}{\partial y} + c(\phi - n)$$
 (2)

In this context,  $\mu_D$  represents the diffusion coefficient across the field, and  $\mu_{\nu}$  stands for kinematic viscosity. The term  $\Gamma$ , defined as  $\Gamma \equiv -\partial_x \ln{(n_0)}$ , indicates the gradient of plasma density. The Poisson bracket is expressed as:  $[A,B] = \frac{\partial A}{\partial x} \frac{\partial B}{\partial y} - \frac{\partial A}{\partial y} \frac{\partial B}{\partial x}$ . Here, the electrostatic potential  $\phi$  acts as the stream function for the  $E \times B$  velocity, represented by  $\mathbf{u} = \nabla^{\perp} \phi$ , leading to  $u_x = -\frac{\partial \phi}{\partial y}$  and  $u_y = \frac{\partial \phi}{\partial x}$ . Vorticity is described by  $\omega = \nabla^2 \phi$ . The normalization of variables follows [14, 15]. The parameter c, reflecting the electron's parallel response, is given by  $c = (T_e k_{\parallel}^2)/(\mathrm{e}^2 n_0 \eta \omega_{ci})$ , where  $\eta$  denotes electron resistivity and  $k_{\parallel}$  is the effective parallel wavenumber.  $T_e$  is the electron temperature,  $n_0$  is the equilibrium density and  $\omega_{ci}$  is the ion cyclotron frequency. Our DNS simulations used a fully dealiased pseudo-spectral method at a grid resolution of  $N_x \times N_y = 1024^2$  in a double periodic domain of size 64 over 400 eddy turnover times. See [16] for more details.

#### 2.2. Heavy impurity particle model, drag force, relaxation time

The motion of heavy impurity particles within plasma is influenced principally by two forces: the Lorentz force generated by electromagnetic fields and a drag force due to collisions with the surrounding plasma ions. The transfer of momentum with plasma ions happens via the electrostatic potential around the impurity, and the influence of electrons is generally negligible given their significantly lower mass. The equation governing the motion of these heavy impurity particles is given by:

$$m_p \frac{d\mathbf{v}_p}{dt} = \mathbf{F}_{\text{drag}} + \mathbf{F}_{\text{Lorentz}},$$
 (3)

with  $m_p$  and  $\mathbf{v}_p$  respectively being the particle mass and the velocity, which expands to:

$$\frac{d\mathbf{v}_p}{dt} = \frac{\mathbf{u}_p - \mathbf{v}_p}{\tau_p} + \frac{Ze}{m_p} (\mathbf{E} + \mathbf{v}_p \times \mathbf{B}). \tag{4}$$

The characteristic relaxation time  $\tau_p$ , which we derived in our earlier research [17], is given by:

$$\tau_p = \frac{m_p}{\sqrt{m_i}} \frac{6\sqrt{2}\pi^{3/2}\epsilon_0^2}{n_i Z^2 e^4} \frac{T_i^{3/2}}{\ln\Lambda} \,, \tag{5}$$

Here,  $n_i$  represents the density of plasma ions,  $T_i$  denotes the ion temperature, and  $\ln \Lambda$  stands for the Coulomb logarithm. When these quantities are normalized based on the HW framework, the resulting equations describing particle motion are:

$$\frac{d\boldsymbol{v}_p}{dt} = \frac{\boldsymbol{u}_p - \boldsymbol{v}_p}{\tau_p} + \alpha(-\nabla\phi(\boldsymbol{x}_p) + \boldsymbol{v}_p \times \boldsymbol{b}),\tag{6}$$

with the parameter  $\alpha = Zm_i/m_p$ .

The spatial evolution of impurity particles is determined by:

$$\frac{dx_p}{dt} = v_p. (7)$$

Equations (6) and (7) describe the trajectories of impurities within a turbulent plasma environment. We focus on tungsten impurities originating from the surface components of fusion devices such as ASDEX Upgrade [18], EAST [19], and ITER. Tungsten ions are examined across various charge states (Z=3,10,20,60), ranging from low to high ionization, and both their relaxation times and Stokes numbers ( $St=\tau_p/\tau_\eta$ ) are systematically investigated. The Stokes number is a dimensionless parameter that highlights how particles in a fluid flow behave, showing the ratio of a particle's relaxation time,  $\tau_p$ , to the flow's characteristic time,  $\tau_\eta$ . For  $St \ll 1$ , particles track the fluid streamlines closely, but for  $St \gg 1$ , the significant inertia means particles are less influenced by flow variations. The flow's characteristic time is  $\tau_\eta=0.35$ . The parameters for  $\tau_p$  calculation are  $n_i=1\times 10^{19}, {\rm m}^{-3},$   $T_i=0.1{\rm eV}$ , and  ${\rm ln}\,\Lambda=10$ . Table 1 includes the normalized relaxation times and  $\alpha$  for different tungsten ion charge states Z.

TABLE 1. Dimensionless parameters for different values of Z

$\overline{Z}$	3	10	20	60
$\tau_p$	3.20	0.29	0.07	0.01
$\dot{\alpha}$	0.03	0.11	0.22	0.66
St	9.14	0.83	0.20	0.03

### 3. RESULTS

In Fig. 1, we present typical examples of trajectories for both fluid tracers (with St=0) and impurity particles with a range of Stokes numbers, all starting from the same initial position, marked by a green cross. To enhance visual clarity, we extended the periodic computational domain  $[0,64] \times [0,64]$  to reveal uninterrupted view of the particle paths. This method of extending the domain was also applied in our statistical evaluations. Fluid tracers (St=0) and particles with a low Stokes number (St=0.03) display random movements typical of particles advected by a turbulent flow. However, as the Stokes number rises, shifts in particle dynamics are observed. For instance, at St=0.83, particles periodically get caught in certain flow areas before suddenly moving to new locations. For articles with a high Stokes number (St=9.14), their dynamics are predominantly influenced by inertia; they are less affected by the flow dynamics and tend to retain their momentum, resulting in more linear trajectory segments between occasional flow interactions.

The mean square displacement (MSD)  $\langle r^2(t) \rangle$  quantifies the average distance particles travel from their starting position as time progresses. It is mathematically expressed as  $\langle r^2(t) \rangle = \langle |\mathbf{r}(t) - \mathbf{r}(0)|^2 \rangle$ , where  $\mathbf{r}(t)$  denotes the position of a particle at any time t, and  $\langle \cdot \rangle$  represent an ensemble average. Fig. 2 shows the time-dependent evolution of the MSD across various Stokes numbers, underscoring fundamentally different transport dynamics. For fluid tracers (St=0), an initial phase of ballistic motion is observed ( $\langle r^2(t) \rangle \propto t^2$ ), with displacement given by  $\mathbf{r}(t) - \mathbf{r}(0) = \mathbf{v}t$  at early timescales up to t=1. Transitioning to t>10, they exhibit normal diffusion ( $\langle r^2(t) \rangle \propto t$ ), aligning with findings in [14]. Particles with very low inertia (St=0.03) behave nearly identically to fluid tracers. For particles with St=0.20, 0.83, and 9.14, hyperballistic motion ( $\langle r^2(t) \rangle \propto t^\mu$  with  $\mu>2$ ) appears at short times, indicating flow-induced acceleration, where displacement follows  $\mathbf{r}(t) - \mathbf{r}(0) = \frac{1}{2}\mathbf{a}t^2$ , with a as the flow-induced acceleration. Notably, these particles undergo superdiffusive movement ( $\langle r^2(t) \rangle \propto t^\mu$  with  $1<\mu<2$ ) at t>10, different from normal diffusion. Different transport exponents  $\mu$  for various Stokes numbers when t>10 are summarized in Table 2.

Turbulent flow often exhibits superdiffusive transport, usually explained by a mix of trapping in coherent structures and long-distance flight events. We use the Okubo-Weiss criterion, which relies on the decomposition of the fluid velocity gradient, for a precise quantitative assessment of particle trapping within vortical structures [20]:

$$Q = s^2 - \omega^2, \tag{8}$$

where  $s^2=s_1^2+s_2^2$  with,  $s_1=\partial_x u_x-\partial_y u_y, s_2=\partial_x u_y+\partial_y u_x$  and  $\omega=\partial_x u_y-\partial_y u_x$ . Using the threshold  $Q_0=\sqrt{\langle Q^2\rangle}$ , the flow domain is divided into three distinct regions: strongly elliptic regions where  $Q\leq -Q_0$  (dominated by vorticity), strongly hyperbolic regions where  $Q\geq Q_0$  (dominated by deformation), and intermediate regions where  $-Q_0< Q< Q_0$ . In Fig. 3, probability density functions (PDFs) of trapping times in strongly elliptic regions (vortices) for various Stokes numbers are presented. Fluid tracers tend to have longer residence

TABLE 2. The Mean Square Displacement (MSD) exponent  $\mu$ , the trapping time exponent  $\gamma$ , and the Hurst exponents H for the velocity.

$\overline{St}$	0 (fluid)	0.03	0.20	0.83	9.14
$\overline{\mu}$	0.97	0.97	1.10	1.32	1.21
$\gamma$	-1.65	-1.93	-2.63	-3.37	-3.19
H	0.52	0.52	0.55	0.62	0.81

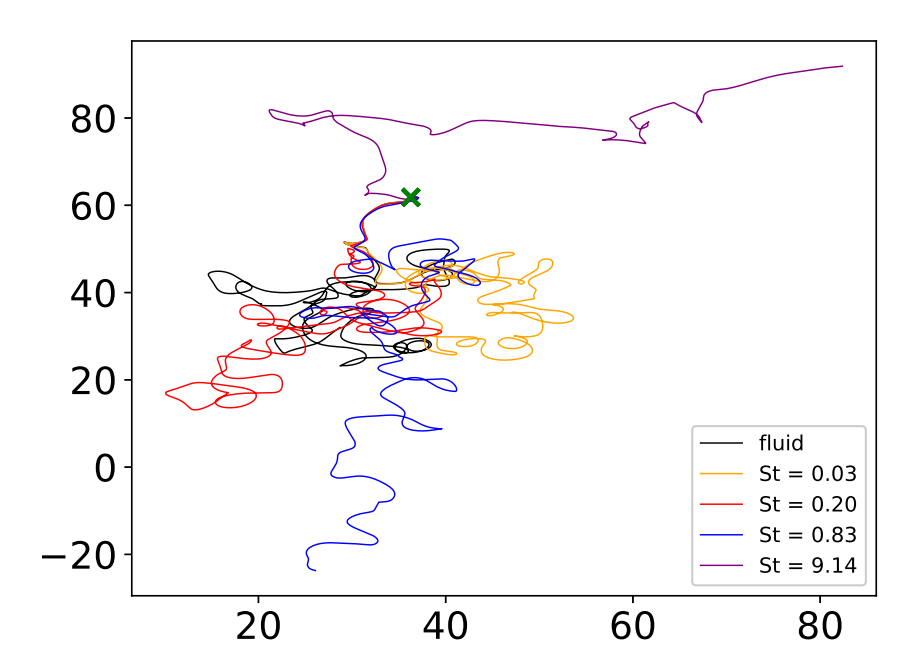


FIG. 1. Trajectories for fluid tracers (St=0) and impurity particles with different Stokes numbers are shown. The periodic domain  $[0,64] \times [0,64]$  has been extended to display continuous trajectories. The common initial position is marked with a green cross.

times, whereas all inertial scenarios demonstrate a more rapid decay, suggesting inertia facilitates particle escape from vortices more effectively. Fig. 3 further reveals a power-law behavior with an exponent  $\gamma$ , with the values listed in Table 2.

The link between trapping time statistics and superdiffusion is a crucial aspect of the fractional kinetics model, which explains anomalous transport in chaotic systems [21, 22]. This theory predicts a direct relationship between the power-law trapping time distribution's exponent  $\gamma$  and the MSD exponent  $\mu$ , expressed as  $\gamma = \mu + 2$  [22]. Our computational results rigorously evaluate this relationship. In situations identified as superdiffusive, our findings align with the theoretical predictions within the range of numerical precision. For instance, for St = 0.83, we obtain  $\mu \approx 1.32$  and  $\gamma \approx 3.37$  (as opposed to the predicted 3.32), and for St = 9.14, we observe  $\mu \approx 1.21$  and  $\gamma \approx 3.19$  (compared to the predicted 3.21). This relation does not apply for nearly diffusive scenarios ( $St \leq 0.20$ ). It is important to note that the reduction in mean trapping time with increasing Stokes number does not confirm superdiffusion, as it could also imply a greater diffusion coefficient in a conventional diffusion process. Yet the  $\gamma = \mu + 2$  relationship serves as a robust consistency check. This specific relationship is characteristic of transport directed by fractional kinetics and is not anticipated in a standard diffusive process. As expected, the relationship holds less accurately for nearly diffusive instances ( $St \leq 0.20$ ), as displayed in Table 2.

In order to gain a deeper insight into superdiffusive behavior, we conducted Hurst analysis on the Lagrangian velocity time series. The well-established Hurst exponent has been a tool for assessing correlations, recognized for its robustness in the presence of random noise [23, 24]. Several methods exist for computing the Hurst exponent, including the R/S method [25]. This technique involves constructing the rescaled range of a time series  $\{V_k, k=1,\ldots,N\}$ , defined as follows:

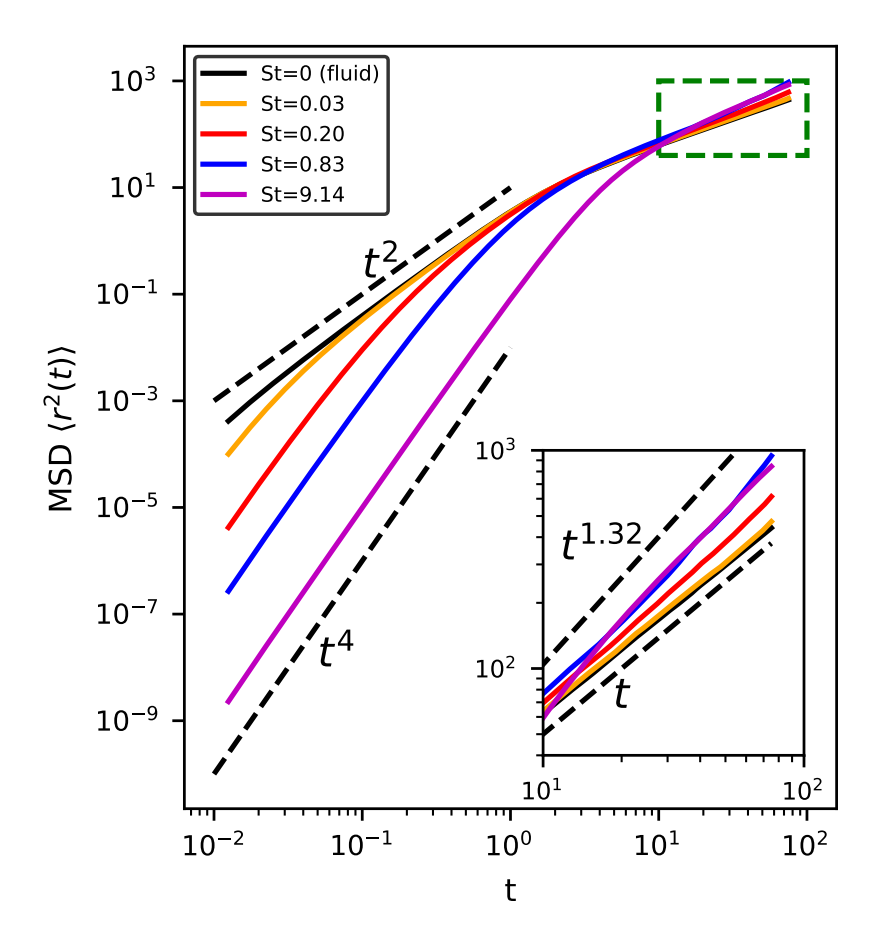


FIG. 2. Mean square displacement versus time for particles with different Stokes numbers. The inset highlights the long-time regime. Fluid tracers (St=0) show ballistic behavior at short times followed by normal diffusion, while particles with higher Stokes numbers exhibit hyperballistic motion at short times and superdiffusive behavior at long times.

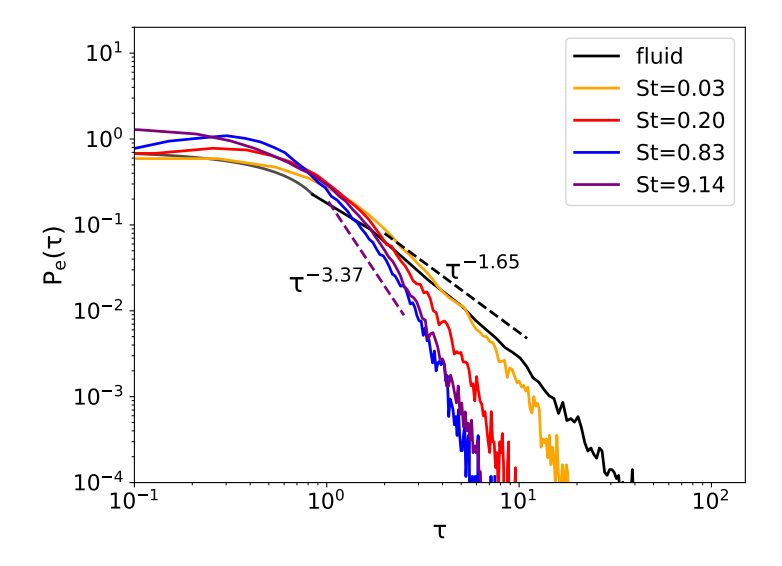


FIG. 3. PDFs of trapping times in strongly elliptic regions (vortices) for particles with different Stokes numbers. Fluid tracers (St=0) show longer trapping times compared to particles with non-zero Stokes numbers, indicating that inertial effects enable particles to escape vortical trapping more easily.

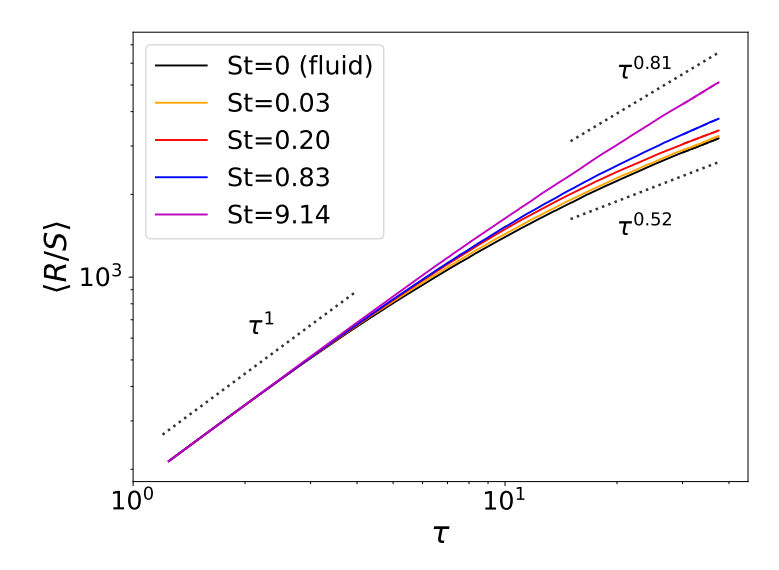


FIG. 4. Log-log plot of the Rescaled Range (R/S) versus time lag  $(\tau)$  for different Stokes numbers.

$$[R/S](\tau) = \frac{\max_{1k\tau} W(k,\tau) - \min_{1k\tau} W(k,\tau)}{\left(\left\langle (V - \langle V \rangle_{\tau})^2 \right\rangle_{\tau}\right)^{1/2}}.$$
(9)

Here,  $W(k,\tau)=\sum_{i=1}^k (V_i-\langle V\rangle_\tau)$  is the cumulative sum of the series after subtracting the mean value, and the denominator represents the standard deviation over the time interval  $\tau$ . The term  $\langle V\rangle_\tau$  denotes the average value of the series  $V_i$  over the time lag  $\tau$ . For a self-similar signal, the rescaled range follows a power law,  $[R/S](\tau)\sim\tau^H$ , allowing the determination of the Hurst exponent, H, from the slope on a log-log plot of [R/S] against  $\tau$ . An exponent of H=0.5 describes an uncorrelated random process typical of normal diffusion, while H>0.5 suggests persistence with positive long-range correlation. Fig. 4 illustrates the R/S analysis for the Lagrangian velocity time series, displaying all Stokes numbers on a log-log scale. At short time lags ( $\tau<10$ ), all curves converge onto a single line with a slope corresponding to a Hurst exponent of approximately  $H\approx 1$ . This shows persistence of the process, where particle velocity remains fully self-correlated over these short intervals. In the long-time asymptotic regime ( $\tau>10$ ), the curves begin to separate, and their slopes, indicative of the long-range Hurst exponent, become influenced by the Stokes number, as summarized in Table 2. The results present a proof of the inertia effect. For fluid tracers with (St=0), we observe  $H\approx 0.52$ , which aligns with the near-random motion typical of a diffusive process. Nevertheless, as the Stokes number grows, the Hurst exponent correspondingly rises, hitting  $H\approx 0.81$  when St=9.14. This consistent increase in H offers quantitative evidence that particle inertia causes long-range persistence in the trajectories of particles.

The autocorrelation function of Lagrangian velocities is examined as well. The autocorrelation is given by  $R(\tau) = \langle \mathbf{v}_p(t) \cdot \mathbf{v}_p(t+\tau) \rangle / \sigma_{v_p}^2$ , where  $\tau$  stands for the time lag and  $\sigma_{v_p}^2$  denotes the variance of particle velocity. The Taylor microscale,  $\tau_{\lambda}$ , which is extracted from the curvature of  $R(\tau)$  at  $\tau=0$ , is defined as  $\tau_{\lambda} = \left(-\frac{1}{2}R''(0)\right)^{-1/2}$ . This microscale indicates the fast decline of correlation near  $\tau=0$  and relates to small vortices within the flow. In Table 3, the values of the Taylor microscale for various Stokes numbers are displayed. It has been noted that  $\tau_{\lambda}$  grows with an increase in the Stokes number, indicating that their velocity correlations degrade slower at small lags, allowing particles to be less affected by rapid fluctuations. High Stokes numbers act like low-pass filters, reducing interaction with smaller eddies. This prevents easy trapping and helps sustain momentum for longer periods, contributing to the persistent motion noted in the Hurst analysis.

TABLE 3. Taylor microscale  $\tau_{\lambda}$  for different Stokes numbers.

$\overline{St}$	0 (fluid)	0.03	0.20	0.83	9.14
$\tau_{\lambda}$	0.46	0.48	0.49	0.52	1.06

### 4. CONCLUSIONS

Our study on the transport of heavy impurities within drift-wave turbulence indicates that the behavior of impurity transport is influenced by the Stokes number. Tungsten impurities with lower charges (associated with high Stokes numbers) and those with intermediate charges (associated with intermediate Stokes numbers) demonstrate superdiffusive transport characteristics. Conversely, tungsten impurities with higher charges (corresponding to low Stokes numbers) exhibit transport patterns similar to fluid tracers, characterized by vortex trapping and normal diffusive behavior over extended time periods. Our findings underscore the importance of inertial effects in driving anomalous transport within fusion plasmas, particularly concerning heavy impurities such as tungsten. These insights are crucial for predicting and understanding impurity transport in fusion systems. The enhanced transport behaviors of lower-charge and intermediate-charge tungsten impurities imply that these species might migrate rapidly through the plasma, enhancing their accumulation in the plasma core and potentially impairing plasma confinement. Subsequent research will extend this investigation to more realistic three-dimensional configurations and introduce two-way coupling to account for impurities' feedback on plasma turbulence.

#### **ACKNOWLEDGEMENTS**

ZL, KS and SB acknowledge the financial support from the French Federation for Magnetic Fusion Studies (FR-FCM) and the Eurofusion consortium, funded by the Euratom Research and Training Programme under Grant Agreement No. 633053. ZL, BK and KS acknowledge partial funding from the Agence Nationale de la Recherche (ANR), project CM2E, grant ANR-20-CE46-0010-01. Centre de Calcul Intensif d'Aix-Marseille is acknowledged for providing access to its high performance computing resources. ZL acknowledges partial financial support from I2M.

#### REFERENCES

- [1] R. A. Pitts et al. "A full tungsten divertor for ITER: Physics issues and design status". *J. Nucl. Mater.* 438 (2013), S48–S56.
- [2] E. M. Hollmann et al. "Status of research toward the ITER disruption mitigation system". *Phys. Plasmas* 22.2 (2015), p. 021802.
- [3] C. Angioni. "Impurity transport in tokamak plasmas, theory, modelling and comparison with experiments". *Plasma Phys. Control. Fusion* 63.7 (2021), p. 073001.
- [4] A. Kallenbach et al. "Impurity seeding for tokamak power exhaust: from present devices via ITER to DEMO". *Plasma Phys. Control. Fusion* 55.12 (2013), p. 124041.
- [5] C Hidalgo. "Edge turbulence and anomalous transport in fusion plasmas". *Plasma Phys. Control. Fusion* 37.11A (Nov. 1995), A53.
- [6] V. Naulin. "Turbulent transport and the plasma edge". J. Nucl. Mater. 363 (2007), pp. 24–31.
- [7] W. Horton. "Drift waves and transport". Rev. Mod. Phys. 71.3 (1999), p. 735.
- [8] R. Sanchez and D. E. Newman. "Self-organized criticality and the dynamics of near-marginal turbulent transport in magnetically confined fusion plasmas". *Plasma Phys. Control. Fusion* 57.12 (2015), p. 123002.
- [9] R. Sánchez et al. "Nature of Transport across Sheared Zonal Flows in Electrostatic Ion-Temperature-Gradient Gyrokinetic Plasma Turbulence". Phys. Rev. Lett. 101 (2008), p. 205002.
- [10] A. Hasegawa and M. Wakatani. "Plasma edge turbulence". Phys. Rev. Lett. 50 (1983), pp. 682-686.
- [11] S J Camargo et al. "Resistive drift-wave turbulence". Phys. Plasmas 2.1 (1995), pp. 48–62.
- [12] Z Lin et al. "Synthesizing impurity clustering in the edge plasma of tokamaks using neural networks". *Phys. Plasmas* 31.3 (2024).
- [13] S. Futatani et al. "Multiscaling dynamics of impurity transport in drift-wave turbulence". *Phys. Rev. Lett.* 100 (2008), p. 025005.
- [14] W. Bos et al. "Lagrangian dynamics of drift-wave turbulence". *Physica D* 239 (2010), pp. 1269–1277.
- [15] B. Kadoch et al. "Origin of Lagrangian Intermittency in Drift-Wave Turbulence". *Phys. Rev. Lett.* 105 (2010), p. 145001.
- [16] Z. Lin et al. "Tessellation-based analysis of impurity clustering in the edge plasma of tokamaks". *J. Plasma Phys.* 91.1 (2025), E30.

### IAEA-CN-392/2798

- [17] Z. Lin et al. "Multi-scale geometrical Lagrangian statistics of heavy impurities in drift wave turbulence". *Plasma Phys. Control. Fusion* 67.4 (Apr. 2025), p. 045038.
- [18] K. Krieger et al. "Conclusions about the use of tungsten in the divertor of ASDEX Upgrade". *J. Nucl. Mater.* 266 (1999), p. 207.
- [19] J. Yao et al. "Overview of the EAST in-vessel components upgrade". Fusion Eng. Des. 98 (2015), p. 1692.
- [20] J. Weiss. "The dynamics of enstrophy transfer in two-dimensional hydrodynamics". *Physica D* 48 (1991), p. 273.
- [21] G. M. Zaslavsky. "Fractional kinetic equation for Hamiltonian chaos". *Physica D* 76.1-3 (1994), pp. 110–122.
- [22] G. M. Zaslavsky et al. "Self-similarity, renormalization, and phase space nonuniformity of Hamiltonian chaotic dynamics". *Chaos* 7 (1997), p. 159.
- [23] B. A. Carreras et al. "Self-similarity of the plasma edge fluctuations". *Phys. Plasmas* 5.10 (1998), pp. 3632–3639.
- [24] J. A. Mier et al. "Characterization of Nondiffusive Transport in Plasma Turbulence via a Novel Lagrangian Method". *Phys. Rev. Lett.* 101 (16 Oct. 2008), p. 165001.
- [25] H. E. Hurst. "Long-term storage capacity of reservoirs". *Trans. Am. Soc. Civ. Eng.* 116.1 (1951), pp. 770–799.